Organic Electronics 14 (2013) 3460–3471

Contents lists available at ScienceDirect

Organic Electronics

journal homepage: www.elsevier.com/locate/orgel

Electric potential mapping by thickness variation: A new method for model-free mobility determination in organic semiconductor thin films ☆

Johannes Widmer *, Janine Fischer, Wolfgang Tress [1], Karl Leo, Moritz Riede [2]

Institut für Angewandte Photophysik (IAPP), Technische Universität Dresden, 01062 Dresden, Germany

ARTICLE INFO

Article history:
Received 4 June 2013
Received in revised form 22 August 2013
Accepted 12 September 2013
Available online 27 September 2013

Keywords:
Organic semiconductors
Charge transport
Mobility
Thin films
Blend layers
Organic Solar Cells

ABSTRACT

Charge transport, with charge carrier mobility as main parameter, is one of the fundamental properties of semiconductors. In disordered systems like most organic semiconductors, the effective mobility is a function of the electric field, the charge carrier density, and temperature. Transport is often investigated in a space-charge limited current (SCLC) regime in thin film single carrier devices, where an electric current is driven in the direction perpendicular to the surface. Direct evaluation of the current–voltage characteristics, however, is problematic, because parasitic contributions from injection or extraction barriers can falsify results.

Here, we present a novel measurement and evaluation technique for key transport parameters. First, it allows for the direct determination of the potential profile in single carrier devices. It is obtained from a series of steady-state current–voltage measurements from devices with varying thickness ("electric *pot*ential *m*apping by thickness variation", POEM). Second, the data can be evaluated to obtain the effective charge carrier mobility $\mu(F,n)$ as a function of the electric field F and the charge carrier density n. Single carrier transport is achieved by sandwiching the organic material under investigation between equally doped layers, i.e. p-i-p (resp. n-i-n) devices for hole (electron) transport investigations. The POEM concept is validated using drift-diffusion simulation data. It is furthermore experimentally applied to small molecular organic semiconductors, where the hole transport in a blend of zinc phthalocyanine (ZnPc) and C_{60} is characterized. In the measured range of $F \approx (1\text{–}5) \times 10^5$ V/cm and hole densities of approx. $(1\text{–}5) \times 10^{16}$ cm^{-3}, the hole mobility is found to be in the range of $(10^{-7}\text{–}10^{-5})$ cm^2/V s, comprising a pronounced field activation with an activation constant of 0.01 $\sqrt{\text{cm/V}}$. A dependence of the mobility on the charge carrier density in the given range is not observed.

The POEM approach does not require a given mobility function as input, i.e. it constitutes a model-free determination of the effective mobility $\mu(F,n)$. It is especially suitable for semiconductors which require complex mobility models, like hopping or trap-dominated transport in disordered systems, and relatively low mobilities, like e.g. neat or mixed organic semiconductors.

* Corresponding author. Tel.: +49 351 463-34905.
E-mail addresses: johannes.widmer@iapp.de (J. Widmer), leo@iapp.de (K. Leo).
[1] Current address: Biomolecular and Organic Electronics, IFM, Linköping University, SE-58183 Linköping, Sweden
[2] Current address: Clarendon Laboratory, Parks Road, Oxford OX1 3PU, United Kingdom

1566-1199/$ - see front matter © 2013 The Authors. Published by Elsevier B.V. All rights reserved.
http://dx.doi.org/10.1016/j.orgel.2013.09.021

1. Introduction

Organic semiconductors attract scientific and commercial attention, because they are expected to complement classic inorganic electronics on several fields, including photovoltaics, displays, illumination, sensors, and other electronics [1–8]. Charge carrier transport in the active organic semiconductors is one of the key parameters for device design, understanding, and material evaluation. Its characterization is an ongoing challenge, particularly as the number of materials potentially suitable for organic electronics is large and steadily being extended. Device understanding and design – including simulations on several levels of detail [9–11] – rely on accurate material and transport parameters, with the charge carrier mobility being one of the key parameters [12–15]. Efficient characterization of new materials accelerates the development and understanding of new and optimized materials and devices.

The available transport characterization methods include organic field effect transistors (OFET) [16], time of flight (TOF) measurements [17], charge extraction with linear increasing voltage (CELIV) [18] and its extensions [19–21], and space-charge limited current (SCLC) measurements. All methods have their specific features and issues, considering the device geometry which should be the same as for the targeted application, the charge carrier density and field strength, which should be in the relevant range, the required quantity of material for sample preparation, a sophisticated measurement set-up, and/or evaluation steps which are based on stronger or weaker assumptions. For a more detailed overview see Ref. [22].

Our aim is to characterize electron and hole transport separately in thin layers of intrinsic or blend organic semiconductors in the direction perpendicular to the surface and at charge carrier densities, field strengths, and current densities relevant for applications like organic photovoltaics (OPV) or organic light emitting diodes (OLEDs). The characterization is done in a stacked device geometry and with a measurement technique as simple as steady-state current–voltage characteristics. The steps of the evaluation are kept transparent and simple, and are based only on plausible basic assumptions. They are model-free with respect to the transport theory, i.e. it is not necessary to compare the measured characteristics to the result of a model-based calculated characteristic to obtain the mobility. This way, unbiased access is gained to the investigated properties, which is especially the charge carrier mobility.

In the following, the idea for the transport characterization through "electric *pot*ential *m*apping by thickness variation" (POEM) is outlined on the level of an ideal single-carrier device disregarding contacts. This is followed by a short section about the general rules for device design, taking non-ideal contacts and their implications for the validity of the POEM theory into account. To proof the principle of the evaluation method, an established drift-diffusion simulation tool is used to create j–V data in a controlled manner, employing several mobility models. The mobility as a function of field and charge density is calculated from these simulated j–V curves, successfully reconstructing the mobility functions used for the simulations. Finally, we investigate the hole transport in a ZnPc:C_{60} blend layer. The hole mobility is determined experimentally, showing a strong field activation and no resolvable charge density dependence in the investigated range.

2. Theory

We analyze charge carrier transport in a thin symmetric semiconductor layer when a mono-polar – i.e. electron-only or hole-only – electric current is driven perpendicular to the layer surface. Transport is regarded as a one-dimensional problem along the spatial variable x in the direction of current, i.e. perpendicular to the thin film surface area. The thickness d_i of the device corresponds to the channel length and the device area A to the channel cross-section area.

2.1. Space-charge limited current

At low current density, we observe an Ohmic current–voltage (j–V) characteristic which can be understood by the fact that the current is mainly carried by the thermal equilibrium charge carrier density. When increasing the current density j, the charge carrier density n within the semiconductor is increased by additionally injected charges and the current density increases beyond the Ohmic behavior. This situation is characterized by a space-charge density distribution decreasing in the direction of current and commonly referred to as space-charge limited current (SCLC). The current density j is independent of x, and according to the drift transport equation

$$j = e\,n\,\mu F \tag{1}$$

the electric field $F(x)$ is reciprocal to the charge carrier density $n(x)$ and increasing from a very small value at the injection contact towards the extraction contact. The charge carrier mobility is denoted by μ and the elementary charge by e. Throughout this work, the charge carrier density is interpreted as the quantity including all mobile and immobile, i.e. free and – if applicable – trapped charge carriers $n = n^{\text{free}} + n^{\text{trapped}}$, and the mobility is regarded as the effective mobility of all these charge carriers, following Eq. (1).

In the theoretical case of a constant charge carrier mobility μ independent of electric field and charge carrier density, and assuming trap-free transport, the electric field has a square-root shape $F(x) \propto \sqrt{x}$ and the j–V characteristics in this case follow the Mott–Gurney law [23, Section 5]

$$j = \frac{9}{8}\,\varepsilon\varepsilon_0\,\mu\,\frac{V^2}{d_i^3} \tag{2}$$

where ε is the relative permittivity of the semiconductor and ε_0 is the vacuum permittivity.

In the case of a field activated mobility according to

$$\mu = \mu_0 \exp\left(\gamma\sqrt{F}\right) \tag{3}$$

where γ is the field enhancement factor, the j–V characteristics can be approximated according to Murgatroyd [24], [25, Section 6.4] by

$$j = \frac{9}{8}\,\varepsilon\varepsilon_0\,\mu_0\,\frac{V^2}{d_i^3}\cdot\exp\left(0.891\,\gamma\sqrt{\frac{V}{d_i}}\right). \quad (4)$$

In the general case of a qualitatively unknown field dependence and/or charge carrier density dependence of the mobility $\mu = \mu(F,n)$ [11,16,15,26–30], F, n, and the j–V characteristic can not be calculated analytically [31, Section 8.6]. It is assumed that in organic semiconductors, may they be neat or blended, the mobility is generally not constant. Reasons are, among others, the spatial disorder of the molecules, the energetic disorder of the frontier orbitals, the occurrence of traps and impurities in the bulk and at interfaces, re-organization energies, and in the case of blend layers the formation of mixed phases of different molecular species.

A positive F or n dependence of the mobility will generally increase the slope of the j–V characteristics, because with increasing V, also n, F, and consequently μ are increasing. However, it is difficult to separate the field and charge density dependence of μ only from the j–V characteristics. For this reason, a different evaluation method is required to directly determine the spatial distribution of the transport quantities. That can be achieved by comparing the voltage of devices with varying thickness d_i at the same current density j, as will be discussed in the following sections.

In Fig. 1, the simulated electric potentials $\Phi(x)$ within two hole-only devices with different thicknesses d_i are compared at the same current density $j = 655\ \mathrm{mA/cm^2}$. (For this example, constant mobility is assumed; details about the used drift-diffusion simulation will be discussed in Section 4.) Looking at the characteristics of the thicker device (dashed lines), the field F is increasing with square-root shape, and the potential Φ, which is the integral of F, is increasing throughout the device with increasing slope towards the extraction contact, proportional to $x^{3/2}$. The charge carrier density is decreasing from the injection contact $x = 0$ towards the extraction contact $x = d_i$.

Looking at the thinner device (solid lines with points) at the same current density, we highlight that the shape of all three curves is identical to the thicker device, from the injection contact up to the beginning of the extraction layer (shaded range at 370 nm).

In this section, the focus is on the intrinsic layer. The interfaces to the doped layers are not discussed in detail. The doped layers in Fig. 1 are required as boundary conditions in the simulation. Their implications will be discussed in detail in the next section, for the discussion in this section we limit ourselves to the observation that the charge density at the extraction interfaces increases simultaneously to the doping level. Knowing that the conductivity in doped layers is high [32], the potential drop there can be neglected. This is reflected in the simulation by a nearly vanishing field and the potential not changing beyond any value which would be relevant compared to the overall voltage. Further details about the validity of this simplification will be discussed below in Section 3.

In summary, the transport quantities in the intrinsic layer are independent of the device thickness, when regarding the same current density and starting the comparison at the injection contact. This finding is not limited to constant mobility but valid for an arbitrary, e.g. field and charge carrier density dependent, mobility function. It is exploited in the potential mapping approach.

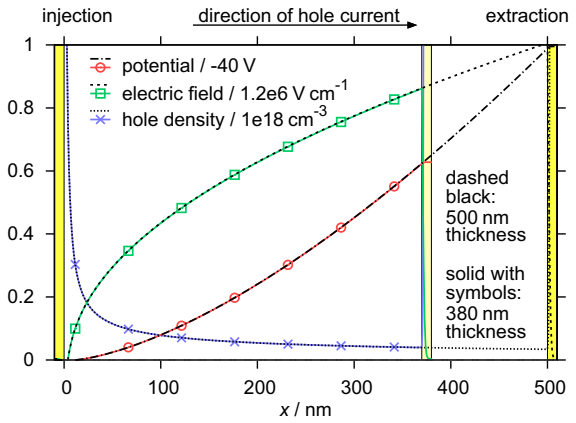

Fig. 1. Electric potential, electric field, and hole density in hole-only devices with two different intrinsic layer thicknesses 500 nm (dashed lines) and 370 nm (solid lines with points) at the same current density of 655 mA/cm^2. The hole mobility in this simulation is 10^{-4} cm^2/V s. The intrinsic layers are symmetrically sandwiched between p-doped injection and extraction layers, illustrated as shaded ranges. The voltage over the whole device is 39.8 V and 25.1 V, respectively. The characteristics are independent of the thickness of the intrinsic layer, in the whole range from the injection contact up to the doped extraction layer.

2.2. Potential mapping

Comparing two devices with different thicknesses d_1 and $d_2 = d_1 + \Delta d_i$, the same current density j is measured at the voltages V_1 and $V_2 = V_1 + \Delta V$. Keeping in mind that the potential $\Phi(x)$ in the range from $x = 0$ to $x = d_1$ is the same in both devices, it can be concluded that the voltage difference ΔV equals the potential difference between the locations $x_1 = d_1$ and $x_2 = d_2$ in the thicker device: $\Delta\Phi = \Phi(x_2 = d_2) - \Phi(x_1 = d_1)$. If this comparison is performed for a large number of thicknesses, it results in a thickness-voltage characteristic for a given current density. It represents a discretized map of the electric potential in the thickest device. The thickness difference Δd_i between the devices is the discretization step width, which has to be small enough to map the curving of the potential. The voltage-thickness characteristic $V(d_i)$ maps the potential $\Phi(x)$ through the mapping equation

$$\Phi(x) = V(d_i) \text{ with } x = d_i. \quad (5)$$

This "electric *pot*ential *m*apping by thickness variation" (POEM) is a direct and model-free experimental access to the spatial distribution of the electric potential at a given current density.

In the following sections, the derivatives of $\Phi(x)$ will be considered. The difference quotient $\Delta V/\Delta d_i$ equals the difference quotient $\Delta\Phi/\Delta x$ at the position $x_1 = d_1$. It can be regarded as the approximate derivative of $\Phi(x)$, if Δd_i is selected small enough to reproduce the curving of the

characteristic, i.e. the approximation of Ohmic behavior ($V \propto d_i$) is valid piecewise. If the curve is interpolated other than linearly, this requirement is irrelevant or has to be adapted to the used algorithm.

2.3. Further evaluation: Field, charge density, mobility

The electric field $F(x)$ can be calculated as the first derivative of $\Phi(x)$. The charge carrier density $n(x)$ can be obtained through Poisson's equation

$$n = \frac{\varepsilon\varepsilon_0}{e} \cdot \frac{\partial F}{\partial x} \tag{6}$$

as proportional to the second derivative of $\Phi(x)$. Assuming drift dominated transport, the charge carrier mobility at any point of the device $\mu(x)$ can be obtained from these quantities through the transport Eq. (1) via

$$\mu(x) = \frac{j}{e\,n(x)\,F(x)} = \mu(F(x), n(x)). \tag{7}$$

According to the last term, the mobility at one position x can be regarded as one value of the field and charge carrier density dependent mobility function $\mu(F,n)$ at the field strength $F(x)$ and the charge carrier density $n(x)$.

2.4. Mobility mapping

The determination of $\mu(x)$ in a certain range $x_{min} < x < x_{max}$ at one current density j results in a 1-dimensional trajectory $\mu(F(x),n(x))$ within the 2-dimensional parameter space of $\mu(F,n)$. Regarding the voltage-thickness characteristics at a different current density, the position of the mapped trajectory of $\mu(F,n)$ is shifted within the parameter space spanned by F and n. The shift takes place in a direction which is generally different from the elongation of the trajectory, i.e. a quasi-two-dimensional surface in the parameter space is covered. Thus, varying both thickness and current density allows for the determination of the mobility $\mu(F,n)$ in a closed area of the parameter space of F and n. In other words: For every set of F and n within the accessible range, one can find at least one current density value, where this set is realised at one point in the device. It can be reconstructed from the voltage-thickness characteristics at this current density. This approach will be demonstrated for simulated model data in Section 4 and applied to experimentally measured data in Section 5.

2.5. Diffusion

Omitting diffusion is a good and practicable approximation in many cases. However, for a more accurate evaluation, it has to be taken into account, extending the transport Eq. (1) by the diffusion term

$$j = e\,n\,\mu F \pm e D n' \tag{8}$$

where $n' = \partial n/\partial x$, which is proportional to the third derivative of $\Phi(x)$, and the positive sign is valid for electrons and the negative sign for holes. D is the diffusion constant, which can be modelled by the classical Einstein relation according to Ref. [33]

$$D = \mu \cdot \frac{k_B T}{e}. \tag{9}$$

With this drift-diffusion model, the mobility can be determined extending Eq. (7) to

$$\mu(x) = \frac{j}{e\,n(x)F(x) \pm k_B T \cdot n'(x)}. \tag{10}$$

In order to model diffusion, the diffusion constant has to be known, which is not always the case, since the validity of the Einstein relation for disordered semiconductors is under discussion [34,35]. When a different diffusion model is appropriate in a specific case, Eq. (10) has to be adjusted accordingly. In the following, diffusion is modelled by the Einstein relation, if not stated otherwise. If diffusion is neglected, the results and conclusions stay valid with only minor deviations.

2.6. Validity and assumptions

Through the presented measurement and evaluation approach, a continuous parameter range of $\mu(F,n)$ is experimentally accessible. The approach is model-free with respect to transport, trapping, and mobility models.

It is valid for energetically ordered and disordered semiconductors, though especially interesting for the investigation of low mobility semiconductors, e.g. organic semiconductors. The latter have the further advantage that devices can be produced via thin-film deposition, allowing for easy variation of the thickness. The method is especially suitable for materials with complex or unknown mobility functions dominating the charge transport. Majority and minority charge carriers cannot be distinguished, thus, the device design must ensure that the minority charge carrier density inside the intrinsic layer is small and their influence, e.g. via recombination, is negligible. This requirement is met in semiconductors with a large energy gap or at low temperature, when the density of thermally generated minority charge carriers is small, and for adjusted work functions (resp. Fermi levels) of the contacts. Beyond that, only the validity of the transport and Poisson's equation have to be assumed, which are generally true. If accounting for diffusion, the appropriate diffusion mechanism has to be known, which might e.g. be given by the Einstein relation (see above) or others, as appropriate for the material system under investigation.

The energy landscape of the semiconductor might or might not contain immobile trap states. In disordered organic semiconductors, transport typically takes place through energetically distributed hopping sites and possible trap sites, with transport being an interplay of charging and discharging of those sites, whereas the differentiation between traps and low-lying hopping sites is often ambiguous. In this work, the resulting mobility is consequently regarded as the average over all charges, regardless of which fraction being trapped or free. In this sense it is an effective mobility. Modelling the charge transport analytically or numerically on the level of lattice or molecules,

charges, and charge transfer processes, an effective mobility $\mu(F,n)$ can be obtained [11,26–28]. The effective mobility function which is measured with POEM can be compared to the effective mobility calculated from these models.

The POEM approach, which was treated theoretically for purely intrinsic material in this section, will be adapted for realistic device geometries in the following section, then verified in simulations, and finally applied experimentally.

3. Device design

The design of device series for POEM measurements should meet several requirements:

- A set of samples with defined device areas, reproducible injection and extraction contacts, and varying but well-known thicknesses of the material under investigation.
- Symmetric device design to avoid a built-in field overlaying the external field.
- Low minority charge carrier density.
- Selective contacts for one kind of charge carriers at both sides, without or with low energy barriers for injection/extraction and with high conductivity of the injection and extraction contacts.
- Stability of the devices at all current densities to be measured and sufficient heat dissipation to avoid electric heating during the measurement.

We realise the contacts by sandwiching the material under investigation between doped layers of constant thickness, where the matrix material is the same material as the material under investigation, and contacting them with equal metal contacts with a suitable work function. This stack results in a p-i-p (p-doped – intrinsic – p-doped) geometry for hole transport investigation, or an n-i-n geometry for electron transport investigation. This stack ensures the symmetry of the device and avoids a built-in field.

Taking the interfaces between the metal, doped, and intrinsic layers as well as a series resistance (e.g. in the substrate) into account does not impair the validity of the potential mapping approach, according to the following reasoning: Charge diffusion from the doped layers into the intrinsic layer leads to an injection and extraction region in the intrinsic layer, with the – generally unknown – thicknesses d_{inj} and d_{extr}. In these regions, the charge carrier density is dominated by the diffusion equilibrium at the interface rather than by charges injected due to the external current. To our experience, in organic semiconductors, their thickness is typically in the order of 10 nm. It can be assumed that at a given current density j, these regions are independent of the device thickness d_i (with $d_i > d_{inj} + d_{extr}$). At the injection contact, this assumption is generally valid (cf. Fig. 1), and at the extraction contact, it is valid as long as the density of injected charges is larger than the density of charges in the equilibrium semiconductor at $j = 0$, which is valid in most cases. It might become invalid for extremely large device thicknesses, low mobilities, and low current densities. In order to account for the injection and extraction zones, the Mapping Eq. (5) has to be extended by the respective offset: $\Phi(x) = V(x + d_{extr})$ for $x > d_{inj}$, where $x = 0$ is defined as the position of the injection interface of the intrinsic layer.

Additionally, a potential drop can occur at the injection and extraction interfaces or in the cables or the contact bars on the substrate. At the injection contact, an energetic injection barrier, e.g. between the metal and organic material, and the level bending at the injection zone might result in a contact voltage V_{inj}. At the extraction contact, a potential drop V_{extr} might occur in the doped layer and at the interface to the metal contact. The voltage drop in the cables/contacts can be summarized as the voltage over a series resistor V_s, which is a function of the electric current $j \cdot A$. All these quantities V_{inj}, V_{extr}, and V_s are depending on the current density, but not on the device thickness d_i. They require the Mapping Eq. (5) to be extended accordingly

$$\Phi(x) = V(x + d_{extr}) - V_{inj} - V_{extr} - V_s \tag{11}$$

with $x > d_{inj}$ and the origin of the voltage axis set to $\Phi(x = 0) = 0$ V. The five quantities d_{inj}, d_{extr},V_{inj}, V_{extr}, and V_s are generally present and their values are unknown. They might be varying when changing the current density, but they are independent of the device thickness when measuring all samples at the same current density. Consequently, they do not impair the validity of the potential mapping. These offsets can further be neglected for the mobility mapping: The voltage offsets are irrelevant, since only the derivatives of $\Phi(x)$ are regarded, and the thickness offsets are irrelevant, too, because they imply a constant shift of the coordinate system of the transport characteristics, leaving the values and trends of the transport quantities unchanged, allowing a still correct $\mu(F,n)$ determination. In summary, a p-i-p or n-i-n stack is suitable for POEM measurements and simulations.

4. Simulation – Proof of principle

Drift-diffusion simulations of single carrier devices are used to validate the POEM evaluation method with well-known model input data. A simulation tool is used, which is based on the differential equation system comprising continuity and diffusion equations for the electron and hole current, as well as Poisson's equation. This differential equation system is solved numerically assuming Boltzmann statistics. Details on the simulation tool can be found in the work by Tress et al., demonstrating also the successful application to device modelling of organic solar cells [9,36].

We simulate hole-only devices with a p-i-p device geometry. The thickness of the doped layers is set to 30 nm, with a doping concentration of 1% of the effective density of states. Small variations of these values do not have a relevant influence on the results. Ohmic contacts are assumed for the interface between the metal contacts and the doped organic layers. Recombination is modelled as bi-molecular recombination according to Langevin theory. The transport gap in the intrinsic layer is modelled

with 2.2 eV, which is a typical value for small molecular organic semiconductors. The temperature is set to $T = 300$ K. The hole mobility in the doped layers and the electron mobility in the whole device are modelled as constant, since they are not in the focus of this work and do not have a relevant influence on the results.

The simulation yields the j–V characteristics of the p-i-p devices, which are then used as input data for a POEM evaluation, trying to reconstruct the hole mobility which was originally used for the simulation. Three different models are applied for the hole mobility in the intrinsic layer μ, which is the focus of this work: (A) Constant mobility; (B) Field activated mobility; and (C) Field and charge carrier density dependent mobility.

4.1. Constant mobility

In the first set of simulations, the hole mobility of the intrinsic layer is modelled with a constant value of $\mu = 10^{-5}$ cm^2/V s.

The current–voltage characteristics obtained in the simulation, see Fig. 2, display two regimes. In the high current regime, the devices approximate the analytically calculated behavior according to the Mott–Gurney law (Eq. (2)). At lower current densities, the simulated curves show a transition to the Ohmic regime. This originates from the equilibrium charge carrier density in the device, resulting from the work function of the electrodes being close to the hole transport level.

The data from a set of simulations with various thicknesses of the intrinsic layer d_i is analysed according to POEM. The value of d_i is varied from 0 nm to 500 nm in steps of 10 nm. As a first step, to obtain the voltage from all devices at one given current density, the current–voltage characteristics from the simulations are interpolated logarithmically[3]. The resulting voltage-thickness characteristics $V(d_i)$ for five exemplary current densities are shown in Fig. 3a (symbols). They are compared to the potential as a function of space from the microscopic output of the simulation with $d_i = 500$ nm (lines). The solid lines show the original data, the dashed lines account for an injection contact voltage of $V_{inj} = 0.2$ V, showing good agreement to the reconstructed data.

In the second step of the POEM evaluation as displayed in Fig. 3b, the derivative of the voltage-thickness characteristics is calculated from the difference quotients of the $V(d_i)$ points, representing the electric field at the respective position. The result (symbols) is plotted together with the field strength calculated by the simulation (lines), showing again good agreement. A small deviation can be observed due to the interpolation of the $V(d_i)$ data from a limited number of simulated voltage points. To ensure smoothness of the consecutive step, a Bézier curve of the reconstructed $F(x)$ is calculated and the smoothed data is used as input for the next step. A Bézier curve is used for smoothing, instead of any fitting to a function, to keep the evaluation model-free.

[3] Linear interpolation on a double-logarithmic scale

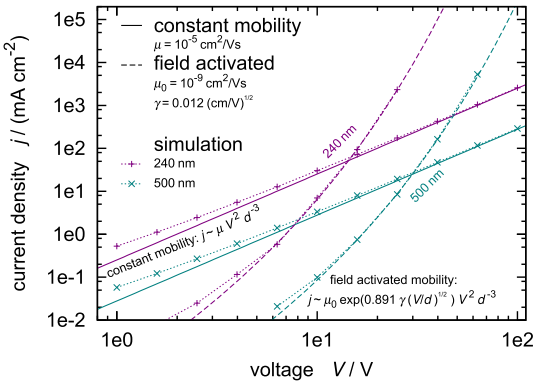

Fig. 2. Simulated and analytically calculated current–voltage characteristics of single carrier devices at two selected thicknesses $d_i = 240$ nm and 500 nm. Solid lines: Mott–Gurney law for a constant mobility of $\mu = 10^{-5}$ cm^2/V s. Dashed lines: Murgatroyd approximation for a field activated mobility with $\mu_0 = 10^{-9}$ cm^2/V s and $\gamma = 0.012\ \sqrt{\text{cm/V}}$. Symbols (connected by dotted lines): Drift-diffusion simulations of p-i-p hole-only devices with the same mobility models.

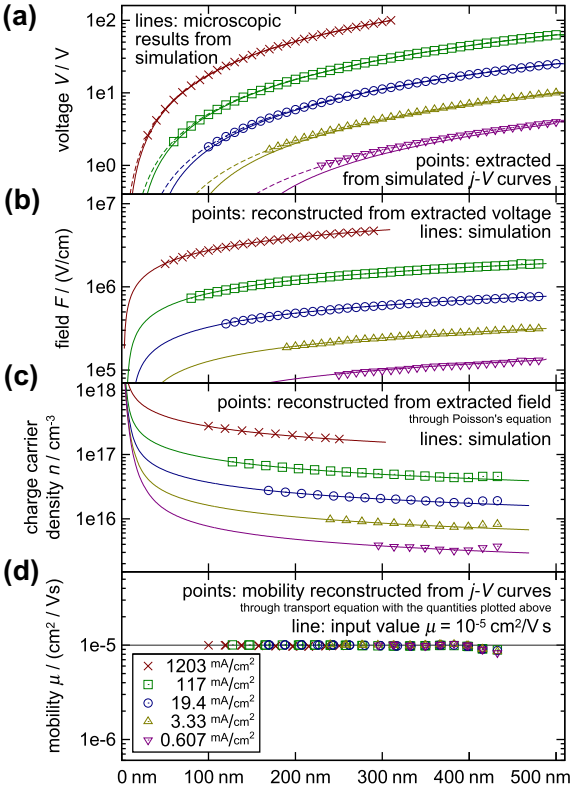

Fig. 3. Step-by-step POEM of a set of simulated single carrier devices with constant mobility $\mu = 10^{-5}$ cm^2/V s. Mobility reconstruction from the j–V curves, at five selected current densities (key in part (d) at bottom left). Symbols show the data extracted from the j–V characteristics of devices with layer thicknesses from 0 nm to 500 nm. Lines show the spatially resolved values from the simulation of a device with 500 nm thickness. (a) Voltage-thickness characteristics extracted from the j–V curves. The dashed lines account for $V_{inj} = 0.2$ V. (b) Field strength: points calculated as the derivative of the points in part (a). (c) Charge carrier density: points calculated according to the Poisson equation from the derivative of the points in part (b). (d) Mobility at each point, reconstructed through the transport equation with the values of the points in parts (b) and (c). The reconstructed mobility successfully maps the original constant mobility of $\mu = 10^{-5}$ cm^2/V s.

In the third step shown in Fig. 3c, the charge carrier density is calculated according to Poisson's Eq. (6), deriving the $F(x)$ data obtained in the previous step. The data is averaged over four points each for further smoothing.

In the final step in Fig. 3d, the mobility μ is calculated through the transport Eq. (1) for every current density and at every point x where both field and charge density data is available, if required through interpolation from two adjacent points. Again, the data is averaged over four points each for smoothing. In all cases, the resulting mobility is very close to the model input value of 10^{-5} cm^2/V s. Deviations are only observed near the end of the evaluable range, which is due to the property of the Bézier algorithm that the end points are overrated compared to the other points of the curve. The reconstructed mobility is independent of the field strength or the charge density, which is in accordance with the mobility used for the simulation. This finding proves that the reconstruction of the mobility from the j–V curves by the POEM evaluation method is successful in the case of a constant mobility.

4.2. Field activated mobility

In the second set of simulations, a field activated model according to Frenkel [37]

$$\mu(F) = \mu_0 \cdot \exp(\gamma\sqrt{|F|}) \tag{12}$$

is used for the mobility, where $\mu_0 = 10^{-5}$ cm^2/V s is the zero field mobility and the exponential factor $\gamma = 0.005\ \sqrt{\text{cm/V}}$ represents the field dependent barrier lowering of a trapped charge carrier in a Coulomb potential. These values are selected as in a typical range for small-molecular organic semiconductors.

The simulated current–voltage characteristics, see Fig. 2, display two regimes, like in the previous example. The low current limit is again Ohmic behavior, the high current limit in this case is the Murgatroyd approximation (Eq. (4)).

The evaluation follows the same scheme as for the previous set of simulations (Subsection 4.1), with Bézier smoothing applied to the $F(x)$ curve. Steps two to four are shown for three selected current densities in Fig. 4. The resulting reconstructed mobility is not constant, but increasing with increasing x and j. The charge carrier density n is identified with the hole density n_h, according to the discussion in Subsection 2.6. To differentiate between a field and hole density dependence, the three-dimensional mobility function $\mu(F, n_h)$ needs to be regarded. For every resulting mobility value at every current density, the field strength and charge density are well-known from the first two reconstruction steps. These values yields one point of the mobility function $\mu(F, n_h)$. All points determined this way are drawn in a 3-dimensional plot (Fig. 5), where the parameters F and n_h are plotted as abscissa and ordinate, and the value of μ is given by the colour around the respective point.

In this chart, the results of the POEM evaluation at 55 different current densities in the value range of (10–5000) mA/cm^2 are plotted. They span the 3-dimensional shape of the mobility function when paying attention to the colour rather than the positions of the points: When moving through the chart horizontally from left to right, the mobility, indicated by the colour, increases. Whereas when moving from bottom to top vertically, it stays constant. These trends can be illustrated by cross-sections through the mobility function, as indicated by horizontal and vertical lines in Fig. 5. In Fig. 6, the resulting characteristics for $\mu(F)$ (left) and $\mu(n_h)$ (right) are shown, plotted as symbols. They are compared to the original mobility

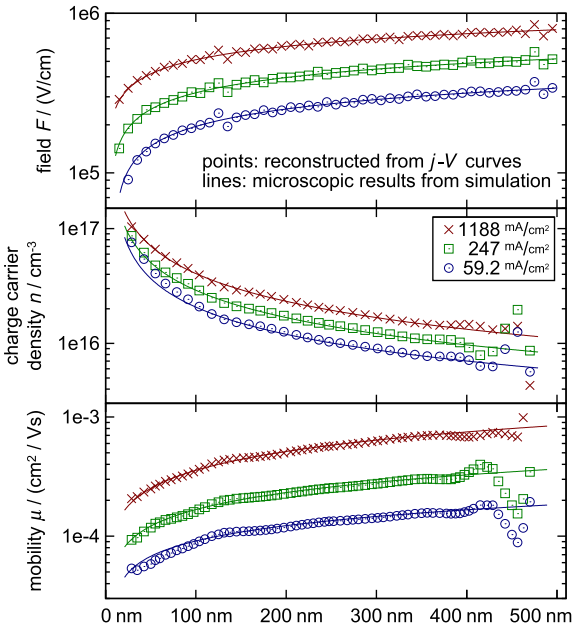

Fig. 4. POEM of a set of simulated single carrier devices with field activated mobility. The evaluation follows the same scheme as described in Fig. 3. Deviations are observed near the end of the evaluable range, which is due to inaccuracies of the interpolated values from the j–V curves and the property of the Bézier algorithm that the end points are overrated compared to the other points of the curve. For the further evaluation, only the points between 60 nm and 350 nm are used.

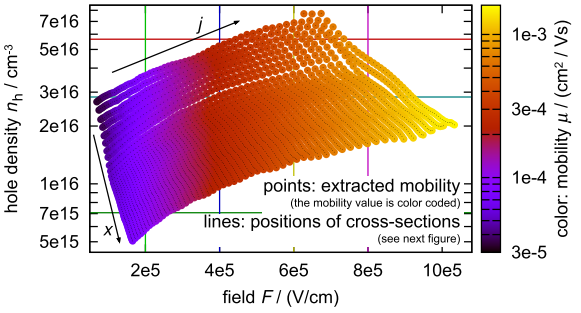

Fig. 5. Mobility reconstructed from the j–V curves of a simulation of single carrier devices with field activated mobility. The data is obtained according to Fig. 4 at 55 different current densities. Each reconstructed point is plotted at the position of the corresponding field strength (abscissa) and hole density (ordinate), surrounded by a grey/colour shade corresponding to the mobility value (scale at right side, brighter colour corresponds to higher mobility). Cross-sections through the mobility function at constant charge density (horizontal lines) and constant field (vertical lines) are shown in Fig. 6.

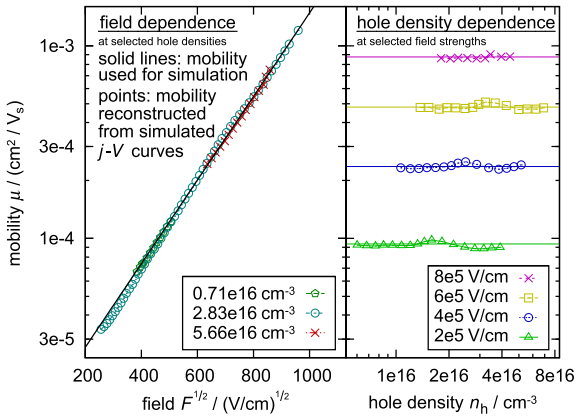

Fig. 6. Mobility reconstructed from the simulated j–V curves of single carrier devices with field activated mobility. The field dependence is shown in the left part, the charge density dependence in the right part of the chart. The mobility axis is valid for both parts. The plotted data points are interpolated values from the data shown in Fig. 5, along the respective cross-sections. Solid lines show the original mobility used as input for the simulation. The reconstructed mobility (points) agrees well with the input mobility for all sets of parameters. The trends (strong field activation, no charge density dependence) can be distinguished and quantitatively resolved.

function $\mu(F)$ (Eq. (3)), plotted as lines, which was used as the mobility model for the simulation of the j–V curves. This mobility function does not include a charge density dependence, but a positive field dependence. Both trends can be seen in the data reconstructed by POEM: Both the field activation and the invariance with respect to the charge carrier density can be resolved, and the resulting values agree well with the model data.

4.3. Field and charge carrier density dependent mobility

In the third set of simulations, a field and charge density dependent model as suggested by Pasveer et al. [28] is used for the mobility. The parameter for the zero-field infinite-temperature limit of the mobility is chosen as $\mu_0 = 10^4$ cm^2/V s, the width of the Gaussian energetic disorder $\sigma = 0.1$ eV, and the lattice constant $a = 1$ nm. The simulation and evaluation are along the lines of the previous paragraph. The resulting reconstructed mobility function is shown (points) and compared to the original model (lines) in Fig. 7. Also in this set, both the field and the density dependence, and the absolute values of the mobility that were assumed for the simulation can be successfully reconstructed and resolved from the j–V characteristics.

As a conclusion, a field dependence and a charge density dependence of the mobility can be distinguished from the j–V curves of a series of single carrier devices with varying thicknesses through the POEM method.

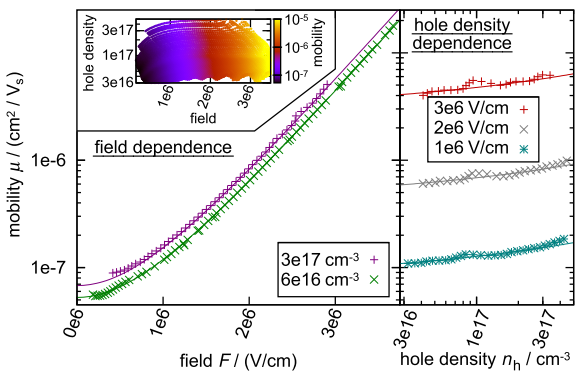

Fig. 7. Mobility reconstructed from the simulated j–V curves of single carrier devices with field and charge density activated mobility. The field dependence is shown in the left part, the charge density dependence in the right part of the chart. The mobility axis is valid for both parts. Solid lines show the original mobility used as input for the simulation. The reconstructed mobility (points) agrees well with the input mobility for all sets of parameters. The reconstructed two-parameter $\mu(F, n_h)$ function is shown as inset (same units as in the large plots).

5. Experimental: Hole transport in ZnPc:C_{60}

In this section, the potential mapping approach POEM, discussed in theory and simulation in the previous sections, is applied experimentally to investigate the hole transport in a blend layer of zinc-phthalocyanine (ZnPc; from ABCR; thin film density: 1.55 g/cm^3) and the Fullerene C_{60} (from CreaPhys; 1.63 g/cm^3), a frequently used donor-acceptor material system for organic photovoltaic devices [38–40]. It is suitable for POEM investigations, because it can be deposited by thin film techniques, allowing for fine control over the layer thickness, and the effective mobility in the blend is expected to be not constant [11]. The two materials are mixed during vacuum deposition on an unheated substrate with a volume ratio of 1:1, showing a phase separation on the scale of few tens of nanometers, creating an interpenetrating network [2]. The effective gap between the HOMO of ZnPc and the LUMO of C_{60} is approx. 1.1 eV [41]. The transfer of holes from C_{60} to ZnPc is known to be fast and efficient, because the HOMO of ZnPc ($-$ 5.1 eV) [42,43] is approx. 1.3 eV higher in energy than the HOMO of C_{60} ($-$ 6.4 eV) [44,45]. As a consequence, the hole conduction in the blend is expected to take place predominantly on ZnPc molecules.

The blend layer thickness is varied from $d_i = 170$ nm to $d_i = 350$ nm in steps of 10 nm. It is sandwiched between 30 nm p-doped layers of ZnPc doped with 2 wt.% (weight-percent) of 2,2-(perfluoronaphthalene-2,6-diylidene) (F6-TCNNQ; see Refs. [46,47]). Injection of electrons can be efficiently suppressed with the C_{60}-free p-doped ZnPc layers [48], and thermally generated electrons have only small Ohmic or weaker contribution to the j–V characteristics, which means negligible contribution to space-charge limited currents. Devices are fabricated on glass substrates and sandwiched between 10 nm thin gold electrodes which are complemented by an additional thicker silver layer to obtain higher conductivity.

All materials including the metals are deposited by thermal evaporation in high vacuum at a base pressure of approx. 10^{-7} mbar. Materials are purified by vacuum gradient sublimation prior to device fabrication, except for the dopant, which is used as received. Contacts are deposited through shadow masks to form bottom and top metal

contact stripes overlapping orthogonally, where the geometric overlap area defines the active device area. Contact stripe widths are varied to achieve three different – approximately square shaped – device areas in the range $A = (0.88–6.44)\ \mathrm{mm}^2$ for every thickness d_i. This variation of A allows for the verification that edge or corner effects are negligible and that the current is proportional to the nominal device area, i.e. the current density j is independent of the device area. The layer thickness is monitored with a quartz crystal micro-balance. Mixed and doped layers are deposited by co-evaporation of two materials with separate thickness monitors. The large number of samples with varying intrinsic layer thicknesses is produced in a wedging process, i.e. fabricating all samples on one large substrate, covering variable parts of it with a metal plate during step-wise deposition of the intrinsic layer. This way, the material consumption for all devices together is only as high as for the thickest device. Current–voltage characteristics are measured at room temperature with a Keithley 2400 source measure unit. The measurement speed is in the range of 0.5 s per voltage point. At high current densities, device self-heating, i.e. Joule heating, through the electric current and possible consequent device break-down limit the achievable current density [49]. Comparing j–V curves measured in DC mode with pulsed j–V measurements using voltage pulse lengths down to 200 μ s, this self-heating effect could be excluded in the investigated devices for current densities below $20\ \mathrm{mA/cm}^2$.

The area variation of the devices allows for checking the proportionality of current and area, and thus, the validity of the current density determination. Data from three devices with the same thickness $d_i = 170$ nm, but different device areas is shown in Fig. 8. While in the Ohmic regime, the current density is different for every device, indicating edge and/or corner effects contributing to current, the current density is independent of the device area in the space-charge limited region (above approx. $0.5\ \mathrm{mA/cm}^2$). This threshold is reached earlier in thicker devices. Current densities in the range of $j = (0.154–19.1)\ \mathrm{mA/cm}^2$ are used for further evaluation, depending on the thickness of the devices.

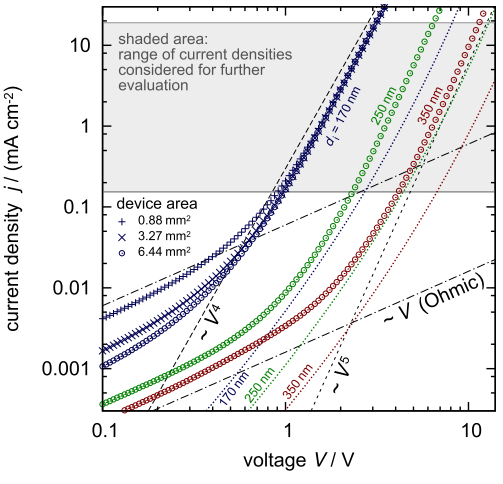

Fig. 8. j–V characteristics of hole-only devices for investigating the transport in ZnPc:C_{60} 1:1 blend. Symbols are measurement results at varying device thickness d_i and device area A. They follow Ohmic behavior in the low-current regime and power-law dependencies in the space-charge limited regime with exponents in the range of 4–5. Black dash-dotted and dashed lines are guides to the eye, representing linear and power-law dependencies. The dotted lines represent the Murgatroyd approximation (Eq. (4)) for the obtained field activated mobility for the same thicknesses as the experimental data.

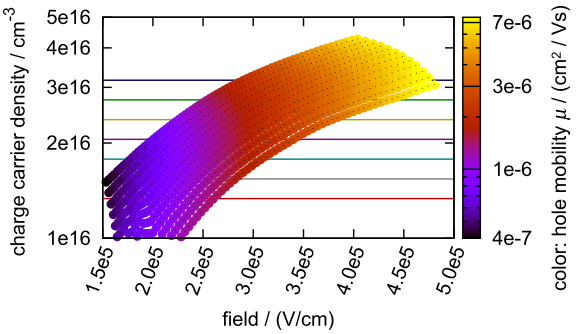

Fig. 9. Hole mobility $\mu(F,n)$ in ZnPc:C_{60} 1:1 blend. The mobility value is coded by the grey/colour scale surrounding each point, where the position of the point indicates the corresponding field strength (abscissa) and charge carrier density (ordinate). A field activation (gradient from dark to bright when going from left to right) can be observed, while a charge carrier density dependence (gradient from bottom to top) cannot be resolved. Cross-sections through the mobility function at constant charge densities (horizontal lines) are shown in Fig. 10.

The j–V curves are analysed according to the POEM evaluation steps discussed above, extracting the $V(d_i)$ characteristics, calculating its derivatives, and reconstructing the mobility function $\mu(F, n_h)$. The plausibility of the evaluation is checked at several stages: The voltage at a fixed current density is increasing with increasing d_i, the field is increasing monotonously, and the charge density is decreasing monotonously with increasing x. Bézier smoothing is applied to the voltage and field curve, the charge carrier density is averaged over two data points.

The result from the mobility reconstruction is shown in Fig. 9. A field activation can be observed, which is visible as a colour gradient from low to high mobilities from left to right, i.e. for increasing field. The parameter range covered by the measurement are field strengths in the range of $(1.5–5.0) \times 10^5\ \mathrm{V/cm}$ and charge carrier densities of $(1–5) \times 10^{16}\ \mathrm{cm}^{-3}$. In this range, a charge density dependence of the mobility cannot be resolved. If any is present, its effect is much weaker than the effect of the field dependence.

The field activation is evaluated quantitatively on the basis of a series of cross-sections of the mobility function at constant charge densities, shown in Fig. 10. It is fitted with Eq. (12), resulting in a zero field mobility of $\mu_0 = 7.9 \times 10^{-9}\ \mathrm{cm}^2/\mathrm{V\,s}$ and a field enhancement factor of $\gamma = 0.01\ \sqrt{\mathrm{cm/V}}$.

5.1. Discussion

The measured field dependence of the hole mobility can be interpreted with the Poole–Frenkel type model as suggested by Gill [37,50]

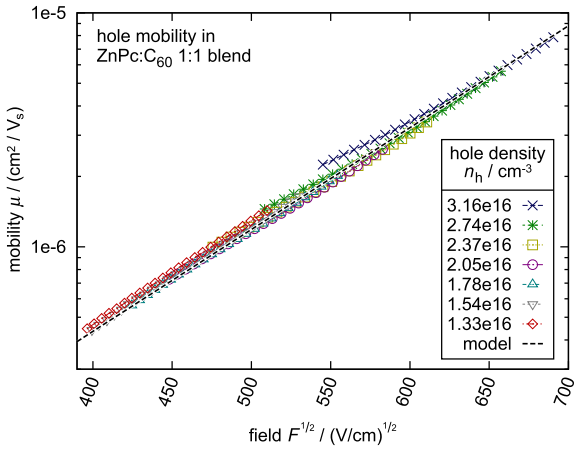

Fig. 10. Field dependence of the hole mobility $\mu(F)$ in ZnPc:C_{60} 1:1 blend, extracted from the mobility function $\mu(F,n)$ (Fig. 9). Each series of symbols indicates the reconstructed field dependent mobility function at one selected charge carrier density. The black dashed line represents a fit of the field activation model $\mu(F) = 7.9 \times 10^{-9}\mathrm{cm}^2/\mathrm{Vs} \cdot \exp(0.01\ \sqrt{\mathrm{cm/V}} \cdot \sqrt{F})$.

$$\mu(F) = \mu_0 \cdot \exp\left(-\frac{\Delta_0 - \beta_{PF}\sqrt{F}}{k_B T_{eff}}\right) \tag{13}$$

$$\text{with} \quad \beta_{PF} = \sqrt{\frac{e^3}{\pi\varepsilon\varepsilon_0}} \text{ and } \frac{1}{T_{eff}} = \frac{1}{T} - \frac{1}{T_0}$$

where Δ_0 is a parameter accounting for the thermal activation, which in our case is set to zero, since temperature variation is not measured, $\varepsilon = 4.7$ is the permittivity of ZnPc:C_{60} 1:1 measured by impedance spectroscopy [51], and ε_0 is the vacuum permittivity. T_{eff}, the effective temperature, is the free parameter for field activation. The result from the fit is $T_{eff} = \beta_{PF}/(\gamma \cdot k_B) = 406$ K (i.e. $T_0 = 1150$ K).

For the microscopic understanding, it should be noted that the dielectric constant of the ZnPc:C_{60} blend is not necessarily the effective dielectric constant for the field activation of the mobility. Since hole transport is expected to take place from ZnPc to ZnPc molecules, in Eq. (13) the value for ZnPc $\varepsilon = 4.0$ might be used rather than the value for the blend. This would change the resulting effective temperature to 445 K.

The Poole–Frenkel model is in agreement with the observed field activation in the measured range, suggesting that molecular hopping, trapping, or some other kind of spatial confinement (e.g. micro-crystallites) for charge carriers in the energy landscape of the transport level is dominating the hole transport in the ZnPc:C_{60} blend. The effective barriers between the confined sites are lowered by the electric field, increasing the mobility with increasing field strength. This Poole–Frenkel model is appropriate for Coulomb-like barriers of heights and distances between the sites which are larger than the range of the binding force. The last criterion is probably not fulfilled, since the typical hopping site distance might be down to molecular dimensions, which are in the order of 1 nm, while the barrier lowering and typical Coulomb interactions take place on a scale of (10–15) nm [37,52].

The measured field dependence of the hole mobility can also be understood based on the Bässler model, attributing the field enhancement to spatial and energetic disorder of the localised hopping sites [26]. However, this model requires a temperature dependent measurement $\mu(F,n,T)$ to quantitatively obtain the relevant parameters.

Space-charge limited current characteristics of trap-dominated transport are expected to yield j–V characteristics with power-law behavior similar to the measured curves [53, Section 4.7] However, the thickness dependence of the exponent can not be explained by this model.

In the evaluated range of field strengths $F = (1–5) \times 10^5$ V/cm, the measured mobility is in the range $\mu = (0.3–8) \times 10^{-6}$ cm^2/V s. This is in good agreement with previous CELIV measurements [54]. These values are approximately one order or magnitude lower than in OFET measurements [43]. This difference is not surprising, because OFET measurements are performed in a different device geometry and at essentially higher charge carrier densities and field strengths. The obtained values are also lower than the hole mobility in neat ZnPc, which is in the range of 10^{-3} cm^2/V s [32]. This difference can be attributed to an increased spatial disorder of the molecules [26] and to the fact that hole conduction takes place only on ZnPc molecules in the blend layer. The volume contributing to hole transport is reduced, and with ZnPc and C_{60} forming an interpenetrating network [2], transport cannot take place on the shortest path in space, but has to follow percolation paths reducing the effective mobility [9,11,30].

To check the plausibility of the resulting mobility function, j–V characteristics are calculated based on the Murgatroyd Eq. (4) with the parameters γ and μ_0 obtained above, and compared to the measured j–V characteristics. It is not expected that the original curve can be completely reconstructed, because the injection voltage V_{inj} is an unknown function of j. However, the comparison can yield valuable information about the injection and extraction mechanism. The result is shown in Fig. 8 as dotted lines at the same three thicknesses as the shown measurement results.

The measured current density is much higher than the calculated current density and the thickness dependence is stronger. This deviation might be due to the diffusion of charge carriers and/or dopant molecules – probably during manufacturing – into the intrinsic layer [48]. The effective thickness of the intrinsic layer would be reduced and, thus, the thickness of the space-charge limited zone, i.e. the actual SCLC thickness is essentially smaller than the nominal intrinsic layer thickness. This hypothesis can also explain the stronger thickness dependence of the measured curves compared to the model calculation. Higher mobility values as reported e.g. for copper phthalocyanine (CuPc) blended with C^{60}, obtained from direct fitting of SCLC j–V data to the Murgatroyd equation [55], might be related to the same origin. A related effect of the influence of doped layers on the thickness of an intrinsic interlayer has recently been reported for pentacene [56].

Apart from the absolute values, the slope of the space-charge regime can be approximately reconstructed, indicating that the mobility function determined by POEM yields plausible values. The possible reduction of the

effective intrinsic layer thickness by a constant value for all devices can be treated as an offset to the thickness coordinate and leaves the validity of the POEM results unchanged.

6. Conclusion and outlook

POEM "electric *pot*ential *m*apping by thickness variation" is a measurement and evaluation method for space-charge limited currents in single carrier devices. It is introduced for the transport characterization and mobility determination in thin film organic semiconductors. It is based on the experimental determination of the spatial distribution of the electric potential in a single carrier device. The evaluation yields access to the charge carrier mobility as a function of the electric field strength and the charge carrier density $\mu(F,n)$. For the evaluation it is not required to fit a given mobility model. In this respect it represents a model-free mobility determination. The measurement consists of current–voltage characteristics of a series of devices with varying layer thicknesses, i.e. channel lengths. The evaluation also yields the spatial distribution of the electric field and the charge carrier density in the device. This concept is validated through several sets of simulated j–V curves with given mobility functions, which can be successfully reconstructed in detail only from j–V characteristics.

We have applied this measurement and evaluation technique to the hole transport in ZnPc:C_{60} 1:1 blend, sandwiched between p-doped ZnPc layers to ensure hole-only transport. The mobility of holes in the blend shows a strong field activation according to

$$\mu_h = 7.9 \cdot 10^{-9} \frac{\mathrm{cm}^2}{\mathrm{V\,s}} \cdot \exp\left(0.01\sqrt{\frac{\mathrm{cm}}{\mathrm{V}}} \cdot \sqrt{F}\right) \quad (14)$$

which is compatible with the Poole–Frenkel type field dependence. The measured j–V characteristics show higher current densities than expected from the model calculation, which might be attributed to the effective intrinsic layer thickness being thinner than its nominal thickness, due to diffusion of charge carriers and/or dopant molecules from the doped layers into the intrinsic layer. The thickness and voltage differences between measured and reconstructed j–V curves might be the starting point for more detailed investigation of the interfaces and injection processes.

Generally, POEM can also resolve the charge carrier dependence of the mobility. However, for the investigated material system, no such dependence could be resolved in the measured parameter range.

Since the obtained mobility is an effective mobility, it can be used to test theoretical models for charge transport, comparing the effective mobility predicted from these models to the measured behavior. The required input data can be obtained by complementary methods [51,57,58]. Variations of the investigated materials and the processing parameters [59–61] allow for the direct investigation of their effect on the transport properties.

The results are particularly relevant since the measurement is performed under working conditions (geometry, current densities) which are typical for applications like organic light emitting diodes or organic photovoltaics, where the mobility governs not only charge transport but also charge separation and recombination [62–65].

Acknowledgments

The work is supported by the German Federal Ministry of Education and Research (BMBF) in the framework of the Projects No. 13N9720 (project "OPEG") and No. 03EK3505D (project "LOTsE"), the Heinrich Böll Foundation, and the project "orthophoto" by the European Social Fund and the Free State of Saxony. The authors acknowledge Novaled AG, Germany, for providing dopants.

References

[1] M.A. Green, K. Emery, Y. Hishikawa, W. Warta, E.D. Dunlop, Progress in Photovoltaics: Research and Applications 21 (2013) 1–11.
[2] M. Riede, T. Mueller, W. Tress, R. Schueppel, K. Leo, Nanotechnology 19 (2008) 424001.
[3] M. Riede, C. Uhrich, J. Widmer, R. Timmreck, D. Wynands, G. Schwartz, W.-M. Gnehr, D. Hildebrandt, A. Weiss, J. Hwang, S. Sudharka, P. Erk, M. Pfeiffer, K. Leo, S. Sundarraj, Advanced Functional Materials 21 (2011) 3019–3028.
[4] www.heliatek.com (2013).
[5] S. Reineke, F. Lindner, G. Schwartz, N. Seidler, K. Walzer, B. Lüssem, K. Leo, Nature 459 (2009) 234–248.
[6] M.C. Gather, A. Köhnen, K. Meerholz, Advanced Materials 23 (2011) 233–248.
[7] Z.B. Wang, M.G. Helander, J. Qiu, D.P. Puzzo, M.T. Greiner, Z.M. Hudson, S. Wang, Z.W. Liu, Z.H. Lu, Nature Photonics 5 (2011) 753–757.
[8] S. Steudel, K. Myny, S. Schols, P. Vicca, S. Smout, A. Tripathi, B. van der Putten, J.-L. van der Steen, M. van Neer, F. Schütze, O.R. Hild, E. van Veenendaal, P. van Lieshout, M. van Mil, J. Genoe, G. Gelinck, P. Heremans, Organic Electronics 13 (2012) 1729–1735.
[9] W. Tress, K. Leo, M. Riede, Advanced Functional Materials 21 (2011) 2140–2149.
[10] D. Rauh, A. Wagenpfahl, C. Deibel, V. Dyakonov, Applied Physics Letters 98 (2011) 133301.
[11] L.J.A. Koster, Physical Review B 81 (2010) 1–7.
[12] W. Tress, A. Petrich, M. Hummert, M. Hein, K. Leo, M. Riede, Applied Physics Letters 98 (2011) 063301.
[13] M. Schober, S. Olthof, M. Furno, B. Lüssem, K. Leo, Applied Physics Letters 97 (2010) 013303.
[14] M. Schober, M. Anderson, M. Thomschke, J. Widmer, M. Furno, R. Scholz, B. Lüssem, K. Leo, Physical Review B 84 (2011) 165326.
[15] R. Coehoorn, P. Bobbert, Physica Status Solidi (A) 209 (2012) 2354–2377.
[16] I.I. Fishchuk, A. Kadashchuk, M. Ullah, H. Sitter, A. Pivrikas, J. Genoe, H. Bässler, Physical Review B 86 (2012).
[17] R. Kepler, Physical Review 119 (1960) 1226–1229.
[18] G. Juska, K. Arlauskas, M. Viliunas, J. Kocka, Physical Review Letters 84 (2000) 4946–4949.
[19] S. Bange, M. Schubert, D. Neher, Physical Review B 81 (2010) 1–7.
[20] R. Österbacka, A. Pivrikas, G. Juška, K. Genevičius, K. Arlauskas, H. Stubb, Current Applied Physics 4 (2004) 534–538.
[21] A. Baumann, J. Lorrmann, D. Rauh, C. Deibel, V. Dyakonov, Advanced Materials 24 (2012) 4381–4386.
[22] N. Karl, Synthetic Metals 133-134 (2003) 649–657.
[23] N.F. Mott, R.W. Gurney, Electronic Processes in Ionic Crystals, second ed., Clarendon Press, Oxford, 1940.
[24] P.N. Murgatroyd, Journal of Physics D 3 (1970) 151–156.
[25] S.-S. Sun, N.S. Sariciftci (Eds.), Organic Photovoltaics – Mechanisms, Materials, and Devices, Taylor and Francis Group, LLC, 2005.
[26] H. Bässler, Physica Status Solidi (B) 175 (1993) 15–56.
[27] V. Arkhipov, H. Bässler, Journal of Non-Crystalline Solids 198-200 (1996) 242–245.
[28] W. Pasveer, J. Cottaar, C. Tanase, R. Coehoorn, P. Bobbert, P. Blom, D. de Leeuw, M. Michels, Physical Review Letters 94 (2005) 206601.
[29] C.G. Shuttle, R. Hamilton, J. Nelson, B.C. O'Regan, J.R. Durrant, Advanced Functional Materials 20 (2010) 698–702.

[30] J. Cottaar, R. Coehoorn, P. Bobbert, Physical Review B 85 (2012) 245205.
[31] M. Schwoerer, H.C. Wolf, Organic Molecular Solids, Wiley-VCH Verlag GmbH, Weinheim, Germany, 2006.
[32] B. Maennig, M. Pfeiffer, A. Nollau, X. Zhou, K. Leo, P. Simon, Physical Review B 64 (2001) 195208.
[33] A. Einstein, Annalen der Physik 322 (1905) 549–560.
[34] G.A.H. Wetzelaer, L.J.A. Koster, P.W.M. Blom, Physical Review Letters 107 (2011) 066605.
[35] K. Harada, A. Werner, M. Pfeiffer, C. Bloom, C. Elliott, K. Leo, Physical Review Letters 94 (2005) 036601.
[36] W. Tress, Device Physics of Organic Solar Cells, Ph.D. Thesis, TU Dresden, 2011.
[37] J. Frenkel, Physical Review 54 (1938) 647–648.
[38] C. Tang, Applied Physics Letters 48 (1986) 183–185.
[39] B. Maennig, D. Gebeyehu, P. Simon, F. Kozlowski, A. Werner, F. Li, S. Grundmann, S. Sonntag, M. Koch, K. Leo, M. Pfeiffer, H. Hoppe, D. Meissner, N. Sariciftci, I. Riedel, V. Dyakonov, J. Parisi, J. Drechsel, Applied Physics A: Materials Science & Processing 79 (2004) 1–14.
[40] J. Widmer, M. Tietze, K. Leo, M. Riede, Advanced Functional Materials, 2013.
[41] J. Widmer, K. Leo, M. Riede, MRS Proceedings 1493 (2013b) h06-01.
[42] A.J. Ikushima, T. Kanno, S. Yoshida, A. Maeda, Thin Solid Films 273 (1996) 35–38.
[43] J. Meiss, A. Merten, M. Hein, C. Schuenemann, S. Schäfer, M. Tietze, C. Uhrich, M. Pfeiffer, K. Leo, M. Riede, Advanced Functional Materials 22 (2012) 405–414.
[44] J.X. Tang, Y.C. Zhou, Z.T. Liu, C.S. Lee, S.T. Lee, Applied Physics Letters 93 (2008) 043512.
[45] W. Zhao, A. Kahn, Journal of Applied Physics 105 (2009) 123711.
[46] P.K. Koech, A.B. Padmaperuma, L. Wang, J.S. Swensen, E. Polikarpov, J.T. Darsell, J.E. Rainbolt, D.J. Gaspar, Chemistry of Materials 22 (2010) 3926–3932.
[47] H. Kleemann, C. Schuenemann, A.A. Zakhidov, M. Riede, B. Lüssem, K. Leo, Organic Electronics 13 (2012) 58–65.
[48] S. Olthof, W. Tress, R. Meerheim, B. Lüssem, K. Leo, Journal of Applied Physics 106 (2009) 103711.
[49] A. Fischer, P. Pahner, B. Lüssem, K. Leo, R. Scholz, T. Koprucki, J. Fuhrmann, K. Gärtner, A. Glitzky, Organic Electronics 13 (2012) 2461–2468.
[50] W.D. Gill, Journal of Applied Physics 43 (1972) 5033.
[51] L. Burtone, J. Fischer, K. Leo, M. Riede, Physical Review 87 (2013) 045432.
[52] S. Gledhill, B. Scott, B. Gregg, Journal of Materials Research 20 (2005) 3167–3179.
[53] M.A. Lampert, P. Mark (Eds.), Current Injection in Solids, Academic Press Inc., 1970.
[54] V. Kazukauskas, A. Arlauskas, M. Pranaitis, R. Lessmann, M. Riede, K. Leo, Physica Status Solidi (C) 6 (2009) 2864–2866.
[55] B.P. Rand, J. Xue, S. Uchida, S.R. Forrest, Journal of Applied Physics 98 (2005) 124902.
[56] H. Kleemann, S. Schumann, U. Jörges, F. Ellinger, K. Leo, B. Lüssem, Organic Electronics 13 (2012) 1114–1120.
[57] Y.S. Yang, S.H. Kim, J.-I. Lee, H.Y. Chu, L.-M. Do, H. Lee, J. Oh, T. Zyung, M.K. Ryu, M.S. Jang, Applied Physics Letters 80 (2002) 1595.
[58] J. Schafferhans, C. Deibel, V. Dyakonov, Advanced Energy Materials 1 (2011) 655–660.
[59] K. Suemori, T. Miyata, M. Hiramoto, M. Yokoyama, Japanese Journal of Applied Physics 43 (2004) L1014–L1016.
[60] J. Sworakowski, K. Janus, S. Nespurek, M. Vala, IEEE Transactions on Dielectrics and Electrical Insulation 13 (2006) 1001–1015.
[61] M. Riede, C. Uhrich, R. Timmreck, J. Widmer, D. Wynands, M. Levichkova, M. Furno, G. Schwartz, W. Gnehr, M. Pfeiffer, K. Leo, in: 2010 35th IEEE Photovoltaic Specialists Conference, IEEE, 2010, pp. 000513–000517.
[62] Y. Terao, H. Sasabe, C. Adachi, Applied Physics Letters 90 (2007) 103515.
[63] M.M. Mandoc, L.J.A. Koster, P.W.M. Blom, Applied Physics Letters 90 (2007) 133504.
[64] G. Garcia-Belmonte, J. Bisquert, Applied Physics Letters 96 (2010) 113301.
[65] W. Tress, K. Leo, M. Riede, Physical Review B 85 (2012) 155201.